Supplementary Information

Impact of cerium doping on the peroxidase-like activity of metal–organic frameworks

Yang Gao[a] and Weisheng Liu[*a]

[a] Key Laboratory of Nonferrous Metal Chemistry and Resources Utilization of Gansu Province and State Key Laboratory of Applied Organic Chemistry, Frontiers Science Center for Rare Isotopes, College of Chemistry and Chemical Engineering, Lanzhou University, 73000 Lanzhou, China

* Corresponding author. E-mail: liuws@lzu.edu.cn

S1. Effects of the pH, catalyst dosage, and reaction temperature on the peroxidase activities of the prepared MOFs

The influence of pH was assessed by conducting the catalytic oxidation of TMB in a 0.1 M acetate buffer at a starting pH of 4.0 and adjusting the pH using the required HCl or NaOH solution. The MOF dosage and reaction temperature were maintained at 0.06 mg·mL^{-1} and 20 °C, respectively. The reaction was conducted for 10 min across a range of pH values (3.0–13.0).

The impact of the catalyst dosage was evaluated at constant H_2O_2 and TMB concentrations of 1.8 and 3 mM, respectively, and at a temperature of 20 °C. The MOF dosage ranged from 0.03 to 0.10 mg·mL^{-1}.

The effect of the reaction temperature was explored at fixed H_2O_2 and TMB concentrations of 1.8 and 3 mM, respectively, and at a constant MOF dosage of 0.06 mg·mL^{-1}. The reaction was performed for 10 min across a range of temperatures (15–45 °C).

S2. Detection of H_2O_2

A mixture of TMB (300 μL, 10 mM in DMF) and H_2O_2 (100 μL) at varying concentrations (5–500 μM) was added to a 0.06 mg·mL^{-1} MOF dispersion (2.6 mL) in acetate buffer (pH 4.0 for MOF-NH_2, pH 5.0 for MOF-NO_2). The mixture was incubated for 10 min at 20 °C. Subsequently, the solution was analyzed by UV–Vis spectrophotometry at 655 nm, and the absorbance was plotted against the H_2O_2 concentration. The limit of detection (LOD) was calculated using the formula LOD = KS_0/S.

S3. Detection of ascorbic acid

Solutions of TMB (200 μL, 0.67 mM in DMF), H_2O_2 (100 μL, 0.67 mM), and ascorbic acid at varying concentrations (1–500 μM) were added to a solution of the MOF (2.6 mL, 0.06 mg·mL^{-1}). The mixture was allowed to react for 10 min at 20 °C. Subsequently, the mixture was analyzed by UV–Vis spectrophotometry at 655 nm, and the variation in absorbance (ΔA) with respect to the ascorbic acid concentration (0–500 μM) was plotted. More specifically, ΔA represents the difference between the absorbance values of TMB in the control group and in the sample with ascorbic acid (655 nm absorbance). The LOD was calculated using the formula LOD = KS_0/S.

To assess the effects of potential interfering substances on the results, anti-interference experiments were conducted using 400 μM solutions of K^+, Zn^{2+}, Na^+, L-glutamic acid (Glu), glycine (Gly), L-histidine (His), fructose (Fru), galactose (Gal), glucose and glutathione (GSH) as substitutes for ascorbic acid, with ascorbic acid serving as the selective control. ΔA denotes the difference between the absorbance value of TMB in the control group and in the sample containing ascorbic acid (AA) or the interfering substance at 655 nm.

S4. Verification of ·OH generation

The degradation of methylene blue (MB) to colorless products in the presence of ·OH was used to confirm the generation of ·OH.[1] For this purpose, nanozymes (1 mg·mL^{-1}, 100 μL) were added to an acetate buffer (0.1 M, pH 4.0 for MOF-NH_2 and pH 5.0 for MOF-NO_2, 1 mL) containing H_2O_2 (1 M, 1 mL) and MB (1 mM, 100 μL). The

absorbance of each reaction solution was monitored after 1.5 h.

S5. Computational details

The energy diagram of the reaction was calculated based on the mechanism outlined in Eqs. S1–S4 under acidic conditions:[2]

$$H_2O_2 + * \rightarrow H_2O_2* \quad (S1)$$

$$H_2O_2* \rightarrow OH* + {}^{\bullet}OH \quad (S2)$$

$$OH*+ H^+ + e^- \rightarrow H_2O* \quad (S3)$$

$$H_2O* \rightarrow H_2O + * \quad (S4)$$

S6. Specific activities of the nanozymes

The specific activity (SA), which is defined in enzyme units per milligram of nanozyme, was evaluated at different nanozyme concentrations.[3] The catalytic activity of the nanozyme, b_{nanozyme} (U), was calculated using Eq. (S5),

$$b_{\text{nanozyme}} = V \times (\Delta A/\Delta t)/\varepsilon \times l, \quad (S5)$$

where V is the total volume of the reaction solution (μL), ε is the molar absorption coefficient of TMB (39,000 $M^{-1}\cdot cm^{-1}$), l is the path length of light traveling in the cuvette (cm), A is the absorbance, and $\Delta A/\Delta t$ is the initial rate of change in the absorbance (655 $nm\cdot min^{-1}$).

The SA of the nanozyme, a_{nanozyme} ($U\cdot mg^{-1}$), was calculated using Eq. (S6),

$$a_{\text{nanozyme}} = b_{\text{nanozyme}}/[\text{m}], \quad (S6)$$

where [m] is the nanozyme weight (mg) in each assay.

S7. Determination of AA in beverages[14]

The beverage sample (Nongfu Spring C100, AA = 22.47 mg/100 mL) was filtered and diluted with ultrapure water 10 times for testing. Briefly, an aliquot of the MOF suspension (200 μL, 200 mg/L; Ce-doped MIL-101(Fe)-NH_2 (1:1.20)), oxTMB (1 mL, 72 μM; converted from TMB), and the sample solution (200 μL) were sequentially added to a 2 mL PE centrifuge tube. After thorough mixing and incubation at 25 °C for 10 min, the ultraviolet absorption of the mixed solution was measured immediately.

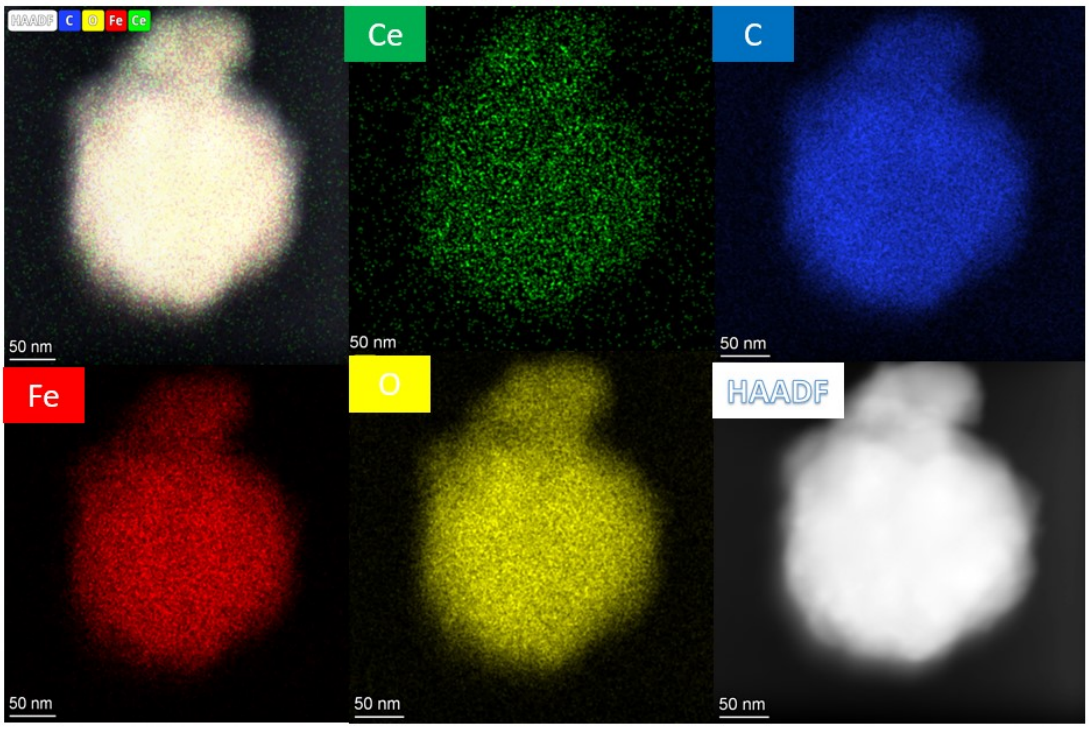

Fig. S1 Elemental mapping of Ce, Fe, C, and O in the Ce-doped MIL-101(Fe)-NH_2 (Ce:Fe = 1:1.20).

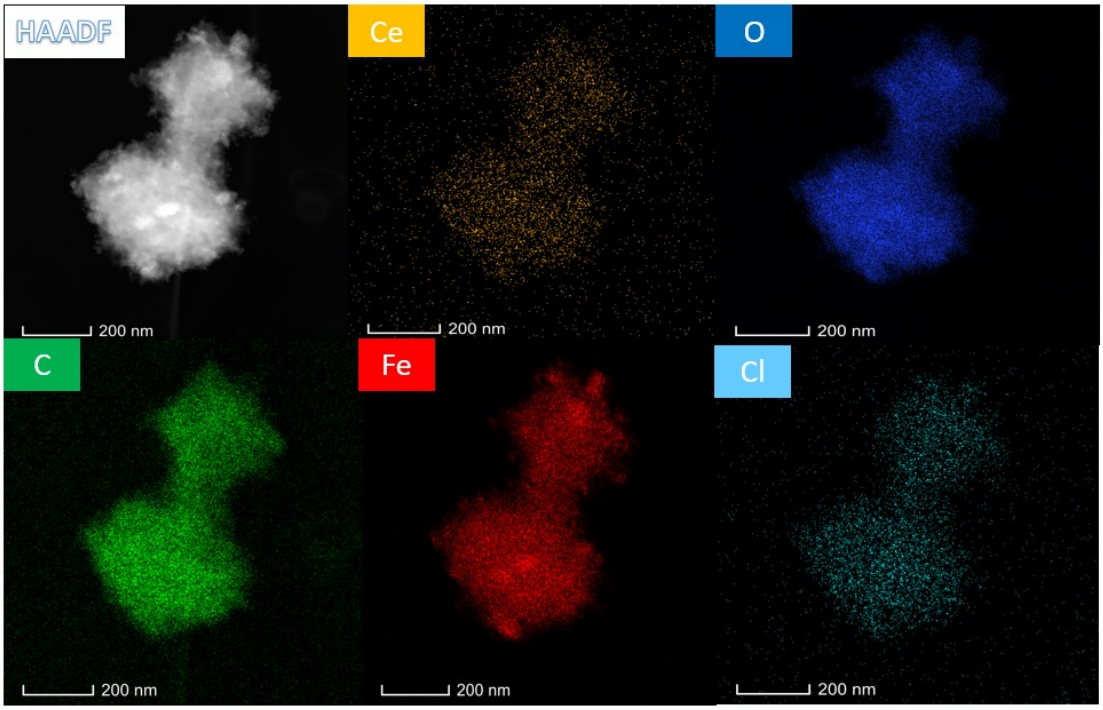

Fig. S2 Elemental mapping of Ce, Fe, C, and O in the Ce-doped MIL-101(Fe)-NO_2 (Ce:Fe = 1:4.17).

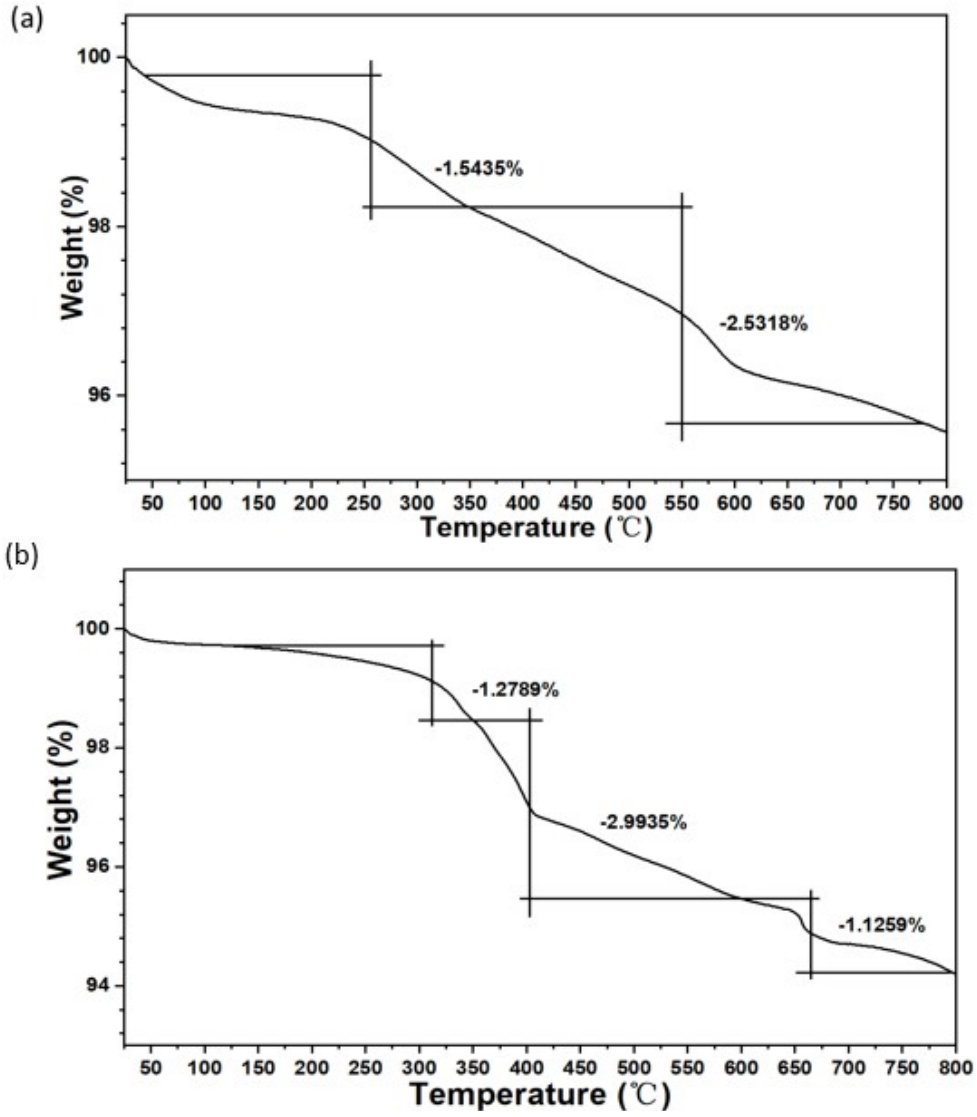

Fig. S3 TGA plots of (a) the Ce-doped MIL-101(Fe)-NH_2 (Ce:Fe = 1:1.20), and (b) the Ce-doped MIL-101(Fe)-NO_2 (Ce:Fe = 1:4.17).

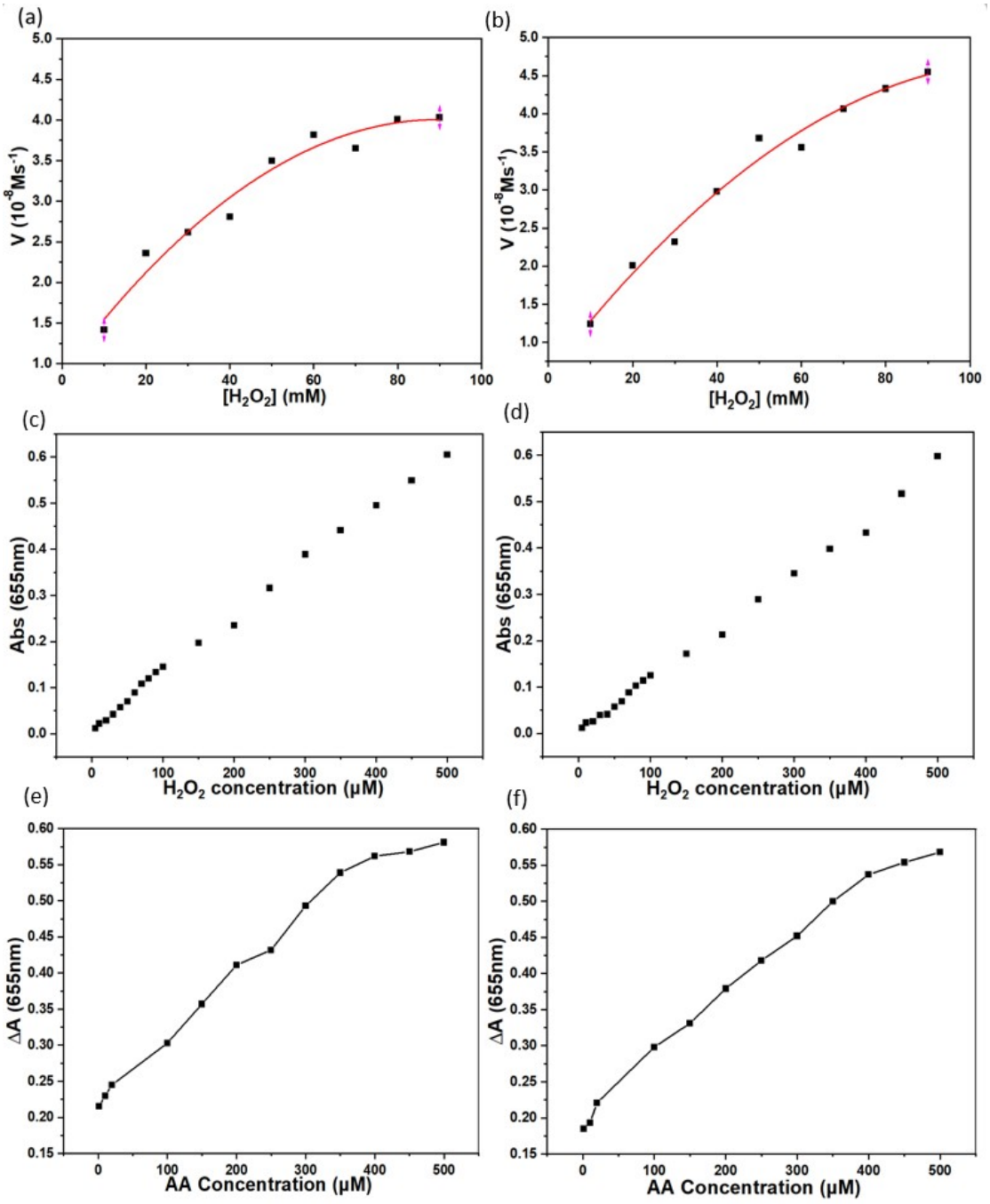

Fig. S4 Steady-state kinetics for the reaction of TMB with H_2O_2 in the presence of (a) the Ce-doped MIL-101(Fe)-NH_2 (Ce:Fe = 1:20), and (b) the Ce-doped MIL-101(Fe)-NO_2 (Ce:Fe = 1:4.17). The TMB concentration was fixed at 0.3 mM, and the H_2O_2 concentration was varied between 10 and 90 mM. Dose–response curves are presented for the colorimetric detection of H_2O_2 using (c) the Ce-doped MIL-101(Fe)-NH_2 (Ce:Fe = 1:1.20), and (d) the Ce-doped MIL-101(Fe)-NO_2 (Ce:Fe = 1:4.17). Dose–response

curves are also shown for the colorimetric detection of ascorbic acid using (e) the Ce-doped MIL-101(Fe)-NH_2 (Ce:Fe = 1:1.2), and (f) the Ce-doped MIL-101(Fe)-NO_2 (Ce:Fe = 1:4.17).

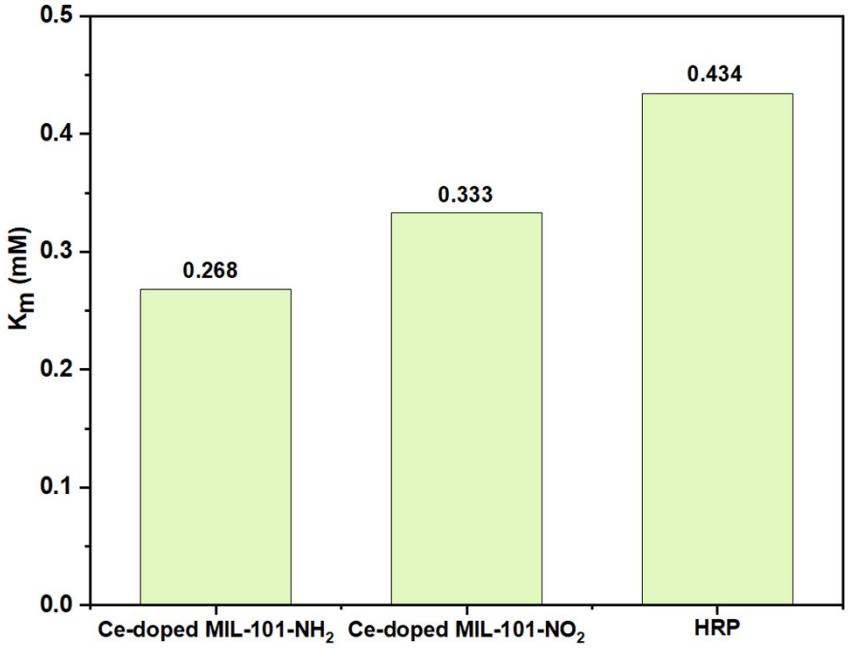

Fig. S5 K_m values determined for the nanozymes during the hydrolysis of H_2O_2.

Table S1 Kinetic parameters for the oxidation of TMB under catalysis by the Ce-doped MIL-101(Fe)-NH_2 (Ce:Fe = 1:1.20) and the Ce-doped MIL-101(Fe)-NO_2 (Ce:Fe = 1:4.17)

Catalyst	K_m (mM)		V_{max} ($M \cdot s^{-1}$)	
	H_2O_2	TMB	H_2O_2	TMB
Ce-doped MIL-101(Fe)-NH_2	26.09	0.268	8.71×10^{-8}	1.84×10^{-8}
Ce-doped MIL-101(Fe)-NO_2	40.75	0.333	6.18×10^{-8}	1.55×10^{-8}

Table S2 Comparison of the K_m and V_{max} values of other peroxidase mimetics

Catalyst	K_m		V_{max} ($M \cdot s^{-1}$)		Ref.
	H_2O_2	TMB	H_2O_2	TMB	
HRP	3.7 mM	0.434 mM	8.71×10^{-8}	10×10^{-8}	4
Se@fMWCNT	——	4.42 μM	——	——	5
Fe-NDs	0.87 mM	0.76 mM	3.76×10^{-8}	2.27×10^{-8}	6
Fe-Al-T	15 mM	0.69 mM	6.93×10^{-9}	2.12×10^{-9}	7
Bi-MOFs	2.5 mM	1.72 mM	0.79×10^{-7}	0.78×10^{-7}	8

Table S3 Ce-doped MOFs and other peroxidase-like sensors for the colorimetric detection of H_2O_2

Colorimetric sensor	LOD	Linearity range	Ref.
Se@fMWCNT	18.23 nM	50 nM–1.4 mM	5
Fe-NDs	0.3 μM	1–60 μM	6
Fe-Al-T	54 μM	10–100 mM	7
Bi-MOFs	0.16 μM	0.5–400 μM	8
Fe_3O_4@AMALG12@Ag	14 μM	0–1250 μM	9
Ce-doped MIL-101(Fe)-NH_2	4.5 μM	5–500 μM	This work
Ce-doped MIL-101(Fe)-NO_2	4.7 μM	5–500 μM	This work

Valence state	Peak	Before catalysis	After catalysis
Fe(II)	Fe(II) Peak 1	18193.66	10383.33
Colorimetric sensor	LOD	Linearity range	Ref.
MVCM	Fe(II) Peak 2 3.57 μM	9199.66 20-500 μM	6985.39 [10]
Fe-P/N–C	Fe(II) Peak 3 0.315 μM	9450.31 0.5–100 μM	5391.75 [11]
Rh SAzymes	Fe(II) Peak 4 0.26 μM	2907.84 10 μM–53.1 mM	2503.28 [12]
Cu NPs/N−$Ti_3C_2T_x$	Total area 0.437 μM	39751.47 5–150 μM	25263.75 [13]
Ce-doped MIL-101(Fe)-NH_2	**Area ratio** 6.1 μM	**51.37%** 1–400 μM	**46.97%** This work
Fe(III)	Fe(III) Peak 1	18481.62	13712.48
Ce-doped MIL-101(Fe)-NO_2	7.2 μM	20–500 μM	This work
	Fe(III) Peak 2	6307.13	5444.32
	Fe(III) Peak 3	9585.23	7113.33
	Fe(III) Peak 4	3252.73	2258.38
	Total area	37626.71	28528.51

Table S4 Ce-doped MOFs and other peroxidase-like sensors for the colorimetric detection of AA

	Area ratio	**48.63%**	**53.03%**

Table S5 Integrated areas of the XPS peaks for Fe ions in different valence states

*From low to high binding energies, the peaks of Fe(Ⅱ),Fe(Ⅲ),Ce(Ⅲ),Ce(Ⅳ) are labeled 1-4,1-4,1-4, 1-6, respectively.

*The peak area has no unit here, because it is a relative strength obtained by integration, not an absolute value.

Table S6 Integrated areas of the XPS peaks for Ce ions in different valence states

Valence state	Peak	Before catalysis	After catalysis
Ce(III)	Ce(III) Peak 1	18714.76	15308.45
	Ce(III) Peak 2	49581.66	55602.38
	Ce(III) Peak 3	12572.26	10293.1
	Ce(III) Peak 4	33231.13	37264.62
	Total area	114099.81	118468.55
	Area ratio	**45.82%**	**46.50%**
Ce(IV)	Ce(IV) Peak 1	18756.91	18460.42
	Ce(IV) Peak 2	31781.4	34436.13
	Ce(IV) Peak 3	29176.45	27629.65
	Ce(IV) Peak 4	13015.95	12834.66
	Ce(IV) Peak 5	22034.99	23870.86

Ce(IV) Peak 6	20133.18	19063.42
Total area	134898.88	136295.14
Area ratio	**54.18%**	**53.50%**

Table S7 Comparison of the feed and actual Ce:Fe molar ratios

Sample		Molar ratio of Ce:Fe	
		#Feeding	ϕReal
MIL-101(Fe)-NH_2		——	——
Ce-BDC-NH_2		——	——
Ce-doped MIL-101(Fe)-NH_2	(Ce:Fe = 1:4)	1:4	1:3.79
Ce-doped MIL-101(Fe)-NH_2	(Ce:Fe = 1:2)	1:2	1:1.88
Ce-doped MIL-101(Fe)-NH_2	(Ce:Fe = 3:4)	3:4	3:3.84
Ce-doped MIL-101(Fe)-NH_2	(Ce:Fe = 1:1)	1:1	1:1.20
Ce-doped MIL-101(Fe)-NH_2	(Ce:Fe = 5:4)	5:4	5:3.75
MIL-101(Fe)-NO_2		——	——
Ce-BDC-NO_2		——	——
Ce-doped MIL-101(Fe)-NO2	(Ce:Fe = 1:4)	1:4	1:4.17
Ce-doped MIL-101(Fe)-NO2	(Ce:Fe = 1:2)	1:2	1:1.92
Ce-doped MIL-101(Fe)-NO2	(Ce:Fe = 3:4)	3:4	3:3.63
Ce-doped MIL-101(Fe)-NO2	(Ce:Fe = 1:1)	1:1	1:0.87
Ce-doped MIL-101(Fe)-NO2	(Ce:Fe = 5:4)	5:4	5:4.15

References

1 Z. Wang, Y. Zhang, E. Ju, Z. Liu, F. Cao, Z. Chen, J. Ren and X. Qu, *Nat. Commun.* 2018, **9**, 3334.

2 W. Xu, Y. Kang, L. Jiao, Y. Wu, H. Yan, J. Li, W. Gu, W. Song and C. Zhu, *Nano-Micro Lett.* 2020, **12**, 184.

3 B. Jiang, D. Duan, L. Gao, M. Zhou, K. Fan, Y. Tang, J. Xi, Y. Bi, Z. Tong, G. F. Gao, N. Xie, A. Tang, G. Nie, M. Liang and X. Yan, *Nat. Protoc.* 2018, **13**, 1506.

4 A. Wu, H. Ding, W. Zhang, H. Rao, L. Wang, Y. Chen, C. Lu and X. Wang, *Food Chem.* 2021, **363**, 130325.

5 L. Gao, J. Zhuang, L. Nie, J. Zhang, Y. Zhang, N. Gu, T. Wang, J. Feng, D. Yang, S. Perrett and X. Yan, *Nat. Nanotechnol.* 2007, **2**, 577.

6 V. P. Sruthi and S. Senthilkumar, *J. Mater. Chem. C.* 2024, **12**, 8924.

7 Y. Liu, J. Yan, Y. Huang, Z. Sun, H. Zhang, L. Fu, X. Li and Y. Jin, *Front. Bioeng. Biotechnol.* 2021, **9**, 790849.

8 L. Li, X. Liu, R. Zhu, B. Wang, J. Yang, F. Xu, S. Ramaswamy and X. Zhang, *ACS Sustainable Chem. Eng.* 2021, **9**, 12833.

9 L. Peng, H. Guo, N. Wu, M. Wang, Y. Hui, H. Ren, B. Ren and W. Yang, *Talanta* 2024, **272**, 125753.

10 S. M. Ismail, A. A. Abd-Elaal, F. H. Abd El-salam, F. A. Taher, I. Aiad and S. M. Shaban, *Chem. Eng. J.* 2023, **453**, 139593.

11 M. Fu, F. Xu, J. Yan, C. Wang, G. Fan, G. Song and B Chai, *Colloids Surf. A* 2022, **641**, 128610.

12 Y. Li, R. Javed, R. Li, Y. Zhang, Z. Lang, H. Zhao, X. Liu, H. Cao and D. Ye,

Food Chem. 2023, **406**, 135017.

13 X. Shi, J. Li, Y. Xiong, Z. Liu, J. Zhan and B. Cai, *Nanoscale* 2023, **15**, 6629.

14 J. Huang, C. Shen, H. Gu, G. Wang, P. Zhou, X. Liu, K. Yu, Y. Qin, K. Zhou, J. Zhang and Z. Chen, *ACS Sustain. Chem. Eng.* 2023, **11**, 17472.